Angular distributions of relativistic charged particles in oriented crystals

M. Kh. Khokonov

Kabardino-Balkar State University

(Submitted 26 November 1992)
Zh. Eksp. Teor. Fiz. **103**, 1723–1741 (May 1993)

The angular distribution of fast charged particles passing through oriented crystals is calculated using an equilibrium microcanonical ensemble in phase space. It is shown that such angular distributions can be used to reconstruct the phase-space distribution with high accuracy. Detailed calculations are carried out for ultrarelativistic electrons, and the influence of electromagnetic radiation on the angular distributions is studied in detail. It is shown that in a number of cases radiation-induced self-focusing of the beam can take place.

1. INTRODUCTION

The angular distribution of fast charged particles resulting from their passage through a disordered medium is a result of a large number of uncorrelated deflections by individual atoms. The corresponding theory for this process is rather well developed, especially for the case of small-angle scattering (see the review[1] by Scott). However, when a beam with a certain initial angular divergence $\Delta < \vartheta_L$ (where ϑ_L is the Linhard critical angle) is incident on the crystal parallel to an atomic chain (or plane), the successive correlated small-angle deflections that determine the transverse trajectory of the particle become important. In order to describe this type of scattering, Linhard[2] introduced a continuous potential for an atomic chain (plane) that depends only on the coordinates transverse to the chain (plane). In this case, the motion of the particle is determined by coherent scattering from the continuous potential, which preserves the transverse energy, and by incoherent scattering from individual atoms. Theoretical analysis shows[3–5] that the first type of scattering leads to the appearance of "rings" (i.e., "doughnut scattering") in the angular distributions. These ring-like angular distributions, which are easy to observe experimentally,[6–8] appear when the beam of particles is incident on the crystal at an angle $\vartheta \geqslant \vartheta_L$ to the atomic chain. Multiple scattering leads to additional smearing of the rings. When the beam penetrates sufficiently far into the crystal the angular distribution of output electrons becomes azimuthally symmetric; the subsequent evolution of this distribution as a function of depth is determined only by incoherent scattering, which changes the transverse energy.

The topic of this paper is the analysis of the distinctive features in the angular distribution when the beam incident on the crystal has a given angular divergence possessing azimuthal symmetry with respect to the atomic axis. It is this case that is most often encountered in practice. As will be shown below, the effect of the continuous potential on such a beam is substantial, even when the thickness of the crystal considerably exceeds the characteristic dechannelization depth z_d. For order-of-magnitude purposes, the quantity z_d for electrons can be defined as the depth at which the mean square of the angle for multiple scattering in the amorphous medium

$$\vartheta_R^2 = \frac{z}{L}\left(\frac{E_s}{E}\right)^2, \tag{1}$$

is comparable to the square of the Linhard critical angle ϑ_L^2, where

$$\vartheta_L = \left(\frac{4Ze^2}{dE}\right)^{1/2} \tag{2}$$

Here E is the electron energy, L is the radiation length, $E_s \approx 21$ MeV, Z is the atomic number of the crystal, d is the spacing between atoms in the chain, and z is the depth.

Three factors cause the angular distributions of electrons in oriented crystals to differ from those of amorphous media: (a) the influence of the continuous potential of the axis (or plane); (b) the fact that the cross section for incoherent scattering by an individual atom in the channel is $\approx S_0/S(\varepsilon)$ times larger than in an amorphous medium, where $S(\varepsilon)$ is the transverse area available to an electron with transverse energy ε and S_0 is the area required by a single chain; and (c) the influence of photon radiation during the motion. We will discuss all of these factors in turn in what follows. Our investigation is based on the concept of statistical equilibrium.[2] We will assume that at a given depth z particles with fixed transverse energy ε are uniformly distributed in the transverse phase space; this corresponds to a microcanonical ensemble. The questions of how long it takes to establish statistical equilibrium[2,8] and how the angular distribution evolves during this time will not be discussed in this paper. This time is considerably shorter for electrons than for positively charged particles, due to anharmonic terms in the potential and strong multiple scattering, and corresponds roughly to a single period of oscillations of the transverse motion.

2. PLANAR CASE

If a particle is incident on the crystal at a small angle ϑ_{in} to a crystallographic plane, the corresponding distribution in the transverse phase space at the surface of the crystal is

$$f_0(x, p_x)dxdp_x = \delta(x - x_{in})\delta(p_x - mv\vartheta_{in})dxdp_x, \tag{3}$$

where x is the transverse coordinate perpendicular to the plane, p_x is the projection of the momentum on the x axis, and $m = m_0(1 - v^2/c^2)^{-1/2}$ is the relativistic mass of the particle. After reaching statistical equilibrium the distribution (3) becomes a microcanonical distribution

$$f(x, p_x, \varepsilon)dxdp_x = \delta\left(\varepsilon - \frac{p_x^2}{2m} - U(x)\right)\frac{dxdp_x}{\Omega(\varepsilon)}, \tag{4}$$

 1063-7761/93/050849-09$10.00

where $U(x)$ is the continuous potential of the plane. It can be shown that the density of states $\Omega(\varepsilon)$ in (4) coincides with the period of transverse motion, i.e., $\Omega(\varepsilon) = T(\varepsilon)$. Integration of Eq. (4) with respect to momentum gives the well-known result for the spatial distribution with respect to coordinates x (see Ref. 2).

The spatial distribution of ions is the subject of the review Ref. 8. For the planar case, this particular question was investigated in detail in Refs. 9 and 10, and also in Ref. 11, taking into account multiple scattering. The theory developed in Ref. 12 allows us to trace the evolution of the angular distribution at small depths in a parabolic potential before the system reaches statistical equilibrium.

If we average (4) using the particle distribution function with respect to transverse energy $F(\varepsilon,z)$, we obtain the distribution in the transverse phase space at a depth z:

$$f(x, p_x, z)dxdp_x = \frac{F(\varepsilon = K_x + U(x), z)}{T(\varepsilon = K + U(x))}\, dxdp_x , \qquad (5)$$

where $K_x = p_x^2/2m$ is the transverse kinetic energy.

Integrating (5) over the transverse coordinate determines the distribution with respect to angle ϑ_x relative to the plane, i.e., $p_x = mv\vartheta_x$.

3. AXIAL CASE

The microcanonical distribution for particles with fixed transverse energy has the following form in the four-dimensional transverse phase space:

$$f(\mathrm{r}, \mathrm{p}, \varepsilon)d\mathrm{r}d\mathrm{p} = \delta\left(\varepsilon - \frac{p^2}{2m} - U(\mathrm{r})\right)\frac{d\mathrm{r}d\mathrm{p}}{2\pi mS(\varepsilon)} , \qquad (6)$$

where $\mathbf{r} = (x,y)$, $\mathbf{p} = (p_x,p_y)$ are the transverse coordinates and momenta; $\Omega(\varepsilon) = 2\pi mS(\varepsilon)$, where $S(\varepsilon)$ is the transverse area available to a particle; $U(\mathbf{r})$ is the total continuous potential of the atomic chains; and $d\mathbf{r}d\mathbf{p}$ is the four-dimensional element of phase-space volume. For the above-barrier particles the area is $S(\varepsilon) = S_0$, i.e., the area required by one chain.

Integrating (6) with respect to momentum leads to the well-known result of Linhard[2] for a distribution of particles that is uniform with respect to the coordinates within an allowed region. On the other hand, integrating (6) with respect to position gives us the distribution with respect to momentum for particles with a fixed transverse energy. When the field $U(r)$ of the chain is azimuthally symmetric, this distribution has the form

$$dn(\mathrm{p}, \varepsilon) = \frac{2\pi rpdp}{mS(\varepsilon)U'(r)} , \qquad (7)$$

where $U'(r) = dU/dr$ and $r = r(\varepsilon,p)$ is found from the condition $\varepsilon = p^2/(2m) + U(r)$. The transverse momentum p is related to the angle ϑ with respect to the chain through the equation $p = mv\vartheta$, where $\vartheta = (\vartheta_x^2 + \vartheta_y^2)^{1/2}$.

In what follows we will discuss the angular distributions of ultrarelativistic electrons in more detail. We will assume that particles are channelized when they have negative transverse energy $-U_m < \varepsilon < 0$, where U_m is the depth of the potential well of the chain. At the periphery of the channel the potential has a complex topology, which is determined by contributions from many neighboring chains. For this case, the corresponding equilibrium distribution with respect to momentum will differ somewhat from the azimuthally symmetric distribution (7). Furthermore, the definition of a channelized particle given above will not be entirely unambiguous. In view of this, it is reasonable to assume that an electron is channelized once the transverse region available to it is smaller than the area occupied by a single chain, i.e., $S(\varepsilon) < S_0$. However, we will limit ourselves to the single-chain approximation, and will consider only azimuthally symmetric angular distributions of the form (7).

For a parabolic potential $U(r) \propto r^2$ the distribution with respect to transverse momentum (7) is uniform within the available region in momentum space. That is, there is complete symmetry between the spatial and angular distributions in this case (i.e., the coordinates and momentum enter into the Hamiltonian in the same way). However, for negative particles the real potential of the atomic chain is far from parabolic and the corresponding angular distribution (7) has a sharp maximum when $\vartheta = 0$. Electrons moving close to the chain have a large transverse kinetic energy, and consequently their paths make a large angle with respect to the axis. The region available to an electron with transverse energy ε in the space of angle is determined by the inequality $\vartheta_{\min} < \vartheta < \vartheta_{\max}$, where $\vartheta_{\max}^2 = 2(\varepsilon + U_m)/E$, while $\vartheta_{\min} = 0$ for $\varepsilon < 0$ and $\vartheta_{\min}^2 = 2\varepsilon/E$ for $\varepsilon > 0$, where E is the electron energy.

Under conditions of statistical equilibrium the coordinates and momenta enter into the distribution function $f(\mathbf{r},\mathbf{p},z)$ only in the combination

$$\varepsilon(\mathrm{r}, \mathrm{p}) = \frac{p^2}{2m} + U(r) . \qquad (8)$$

In this case, Eq. (6) implies the relation[13,14]

$$F(\varepsilon, z) = 2\pi mS(\varepsilon)f(\varepsilon, z) , \qquad (9)$$

where $F(\varepsilon,z)$ is the distribution function with respect to the transverse energy.

Taking into account Eqs. (6)–(8), we can write the distribution of particles with respect to transverse momentum in the form

$$\frac{dn(p, z)}{2\pi pdp} = 2\pi\int \frac{r}{U'}\Big|_{r=r(\varepsilon,p)} f(\varepsilon)d\varepsilon , \qquad (10)$$

where $r(\varepsilon,p)$ is found from condition (8).

The contribution from channelized electrons is determined by (10) along with the limits of integration $-U_m + K(p) < \varepsilon < 0$; here and in what follows $K(p) = p^2/(2m)$ is the transverse kinetic energy, which for channelized particles can vary within the limits $0 < K(p) < U_m$. For above-barrier electrons the limits of integration in (10) are

$$\begin{aligned} &0 < \varepsilon < K(p) \quad \text{for} \quad 0 < K(p) < U_m, \\ &-U_m + K(p) < \varepsilon < K(p) \quad \text{for} \quad K(p) > U_m . \end{aligned} \qquad (11)$$

When all this is taken into account, we find that the total distribution with respect to momentum is determined by (10), along with the limits of integration

$-U_m + K(p) < \varepsilon < K(p)$, where now $0 < K(p) < \infty$.

Taking into account relation (8), Eq. (10) can be written in the form

$$n(p, z) = \int_0^{r_0} f(\varepsilon = K(p) + U(r), z) 2\pi r dr , \qquad (12)$$

where $n(p,z) \equiv dn(p,z)/2\pi p dp$, $r_0 = (\pi N d)^{-1/2}$ is the channel radius, N is the density of atoms in the crystal, and d is the spacing between atoms in the chain.

Equation (12) also follows directly from (6); however, the considerations discussed previously allow us to write the angular distribution in terms of the function $F(\varepsilon,z)$, and also to distinguish the individual contributions to the angular distribution from particles with different transverse energies.

For a canonical phase-space distribution of the form

$$f(\varepsilon) = A \exp(-\beta\varepsilon) \qquad (13)$$

we obtain the following distribution with respect to transverse momentum:

$$n(p) = A \exp\left(-\beta \frac{p^2}{2m}\right) \int_0^{r_0} \exp[-\beta U(r)] 2\pi r dr . \qquad (14)$$

Thus, if the distribution of particles in the phase space is canonical, then the corresponding angular distribution is Gaussian, independent of the form of the atomic chain potential. However, the converse does not hold, i.e., if a beam is incident on the crystal along a certain axis with an angular distribution that is Gaussian in form, the initial distribution in phase space at the crystal surface is not canonical. Nevertheless, it will be clear from what follows that multiple scattering redistributes particles in phase space so that the distribution $f(\varepsilon,z)$ may be considered approximately canonical, i.e., in the form (13), even for insignificant thicknesses $z \ll z_d$. In this case, the parameters A and β depend on the depth and type of crystal.

Another important special case is the uniform distribution in phase space of the form

$$f(\varepsilon) = \begin{cases} f_0, & -U_m < \varepsilon < \varepsilon_1 , \\ 0, & \varepsilon > \varepsilon_1 , \end{cases} \qquad (15)$$

where $f_0 = \text{const}$, $\varepsilon_1 > 0$.

According to (12), the angular distribution corresponding to the function (15) will have the form

$$n(p) = \begin{cases} \pi f_0 r_0^2 , & 0 < K(p) < \varepsilon_1 , \\ \pi f_0 r^2(p) , & \varepsilon_1 < K(p) < \varepsilon_1 + U_m , \end{cases} \qquad (16)$$

where $r(p)$ is found from the condition (8) for $\varepsilon = \varepsilon_1$, $K(p) = p^2/(2m)$. The angular distribution (16) is also uniform in the range of angles $0 < \vartheta < (2\varepsilon_1/E)^{1/2}$.

In practice, a uniform phase-space distribution of type (15) is realized in the case where the incident beam has a large angular divergence $\Delta > \vartheta_L$ with a uniform distribution. Then the initial distribution in phase space will also be uniform over a wide range of transverse energies, i.e., $f(\varepsilon, z=0) = \text{const} \cdot \Delta^{-2}$ for $-U_m < \varepsilon < -U_m + E\Delta^2/2$, and then falls rapidly to zero for $-U_m + E\Delta^2/2 < \varepsilon < E\Delta^2/2$.

According to (10) and (12), the axisymmetric angular distribution that results when electrons move in the field of atomic chains can be written in the form

$$n(\vartheta, z) = \pi m v^2 \int \frac{F(\varepsilon = \varepsilon(\vartheta, r), z)}{S(\varepsilon = \varepsilon(\vartheta, r))} r dr , \qquad (17)$$

where $n(\vartheta,z) \equiv dn/2\vartheta d\vartheta$ and $\varepsilon(\vartheta,r) = mv^2\vartheta^2/2 + U(r)$.

The difference between the angular distribution for an oriented crystal and that for an amorphous medium is most noticeable in thin crystals, i.e., for $z \ll z_d$. Here, if a parallel beam of electrons is incident on the crystal along an atomic chain, then according to (17) the angular distribution will have a half-width on the order of the critical angle, i.e., $\delta\vartheta_{1/2} \sim \vartheta_L$, even at depths $z \sim r_0/\vartheta_L \ll z_d$ corresponding to the period of a single oscillation; this greatly exceeds the same quantity in an amorphous medium. Thus, coherent scattering by the continuous potential leads to a significant broadening of the angular distribution.

An electron moving in the field of an atomic chain has another integral of motion, i.e., the angular momentum about the chain $\mu = xp_y - yp_x$. The corresponding theory of dechannelization was discussed in Refs. 15–17. In this case, the equilibrium microcanonical distribution takes the form[18]

$$f(\mathrm{r}, \mathrm{p}, \varepsilon, \mu) = [2\pi T(\varepsilon, \mu)]^{-1} \delta(\varepsilon - \frac{p^2}{2m} - U(r)) \delta(\mu - xp_y + yp_x) , \qquad (18)$$

where $T(\varepsilon,\mu)$ is the period of radial oscillations. Taking (18) into account, the expressions for the angular distributions have a considerably more complicated form than (17). It was shown in Ref. 19 that the distribution in angular momentum of electrons with a given transverse energy becomes uniform at depths $z \sim (a_F/r_0) z_d \ll z_d$ (where a_F is the screening parameter), which allows us to use (6), (7), (10), (12), and (17). We will not include the influence of the angular momentum in what follows.

4. NUMERICAL RESULTS

In order to calculate the angular distributions of electrons while taking into account multiple scattering, we carried out a numerical simulation of the process. In Refs. 15–17 the problem of axial channelization was investigated in the diffusion approximation by the method of kinetic equations. There the angular momentum was taken into account. The approach we have adopted allows us to take into account incoherent large-angle scattering. However, we limit ourselves to the approximation of a uniform distribution with respect to angular momentum.[19] Furthermore, in treating incoherent scattering by individual atoms we limit ourselves to the region where the first Born approximation is applicable. This is permissible for crystals that are not too heavy, for which (see Ref. 20, para. 1.6)

$$\varkappa = 2Ze^2/\hbar v < 1\,. \tag{19}$$

Then for the Møller potential the scattering cross section by an individual atom has the form

$$d\sigma = \sigma_0 \sum_{i,k}^{3} \frac{\alpha_i \alpha_k 2\theta d\theta\, \theta_a^2 D(\theta)}{(\theta^2 + \beta_i^2\theta_a^2)(\theta^2 + \beta_k^2\theta_a^2)}\,, \tag{20}$$

where $\alpha_i = 0.1, 0.55, 0.35$, $\beta_i = 6.0, 1.2, 0.3$ are parameters of the Møller potential, and

$$\sigma_0 = \pi a_F^2 \varkappa^2 \tag{21}$$

is the total scattering cross section for a Coulomb potential with exponential screening (i.e., the Yukawa potential). The Debye–Waller factor

$$D(\theta) = 1 - \exp(-u^2\theta^2/a_F^2\theta_a^2)$$

strongly limits the probability of small-angle scattering, and is associated with our excluding the coherent part of the scattering from consideration; here $\theta_a = \hbar c(Ea_F)^{-1}$ is the characteristic scattering angle for an atom, and u is the average amplitude of thermal oscillations of nuclei in the crystal. The factor $D(\theta)$ in (20) decreases the total scattering cross section by a factor of 2 to 3. Thus, for misaligned silicon the mean free path computed using the exact expression (20) comes to $l_{am} \approx 1$ μm, whereas the simple expression (21) gives $l_{am} \approx 0.4$ μm.

Coherent scattering by the continuous potential limits the transverse region available to an electron with transverse energy ε. This causes the cross section for scattering by the channel to increase by a factor of $S_0/S(\varepsilon)$ in comparison with (20). For the middle of the well ($\varepsilon \approx -0.5U_m$) the ratio $S_0/S(\varepsilon)$ is 30 to 40. An approach analogous to the one described here was used previously by Kunonets and Ryabov[21-23] to calculate the multiple scattering of electrons with energies in the hundreds of GeV. In our case a more precise expression was used for the scattering cross section (20). Beloshitskii *et al.*[24] used the diffusion approximation in their numerical simulation, which is apparently justified at high energies. As in Refs. 21–24, we used the Doyle–Turner approximation as the potential for the atomic chain.[25]

In order to calculate the angular distribution it is often convenient to use a standard potential[2] in the form

$$U(r) = -U_L \ln\left(1 + \frac{Ca_F^2}{r^2 + r_1^2}\right) + U_0\,, \tag{22}$$

where $U_L = Ze^2/d$.

Equation (8) then leads to the following expression for the angular distribution of electrons with a fixed transverse energy:

$$dn(\varepsilon, E, \vartheta) = 2C \frac{a_F^2}{\vartheta_L^2} \frac{e^x}{(e^x - 1)^2} \frac{2\pi\vartheta d\vartheta}{S(\varepsilon)}\,, \tag{23}$$

where $x = (U_0 - \varepsilon)/U_L + 2(\vartheta/\vartheta_L)^2$.

In Fig. 1 we show the results of a calculation of the angular distribution of electrons with energy 1 GeV in ⟨111⟩ silicon with a thickness of 20 μm. The corresponding distribution function in transverse energy is shown in Fig. 2, where the dashed curves show the contribution from electrons with various trajectory angles. A characteristic feature in the angular distribution is the presence of a linear region for $\vartheta < \vartheta_L$. It is clear from Fig. 1 that the choice of the form of the atomic chain potential does not strongly affect the character of the angular distribution except in the region of small angles. The solid curve in Fig. 1 corresponds to a Gaussian distribution (14) for the canonical distribution function in phase space (13) with parameters $A = 0.57\,A_0$, $\beta = 60$ eV, where $A_0^{-1} = 2\pi m S_0 U_L$. The parameters of the potential (22) for silicon are $C = 3.55$, $r_1 = 0.15$ Å. It is clear from Fig. 1 that the simple expression (14) describes the shape of the curve $n(\vartheta, z)$ adequately. The dashed curve

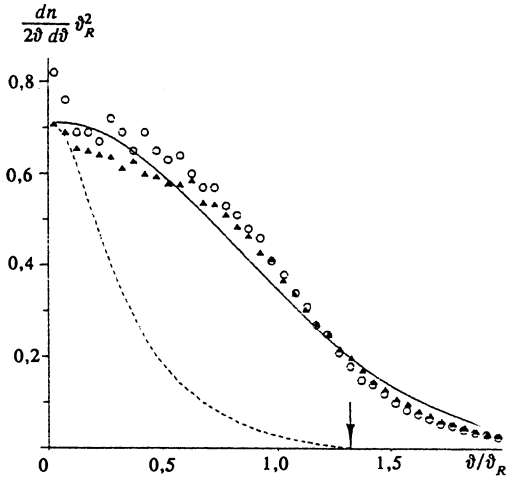

FIG. 1. Angular distribution of electrons with $E = 1$ GeV in ⟨111⟩ silicon with a thickness of 20 μm: ▲—calculation using the Doyle–Turner potential,[25] ○—for the Linhard potential.[22] The solid curve is the Gaussian distribution (14) corresponding to the canonical distribution (13), the dashed curve is the contribution to the Gaussian distribution from channelized particles. The initial beam divergence is $\Delta = 0.2\vartheta_L$. The arrow corresponds to the critical angle ϑ_L [see (2)]. The angles are given in units of $\vartheta_R = 2.9 \cdot 10^{-4}$ rad [see (1)].

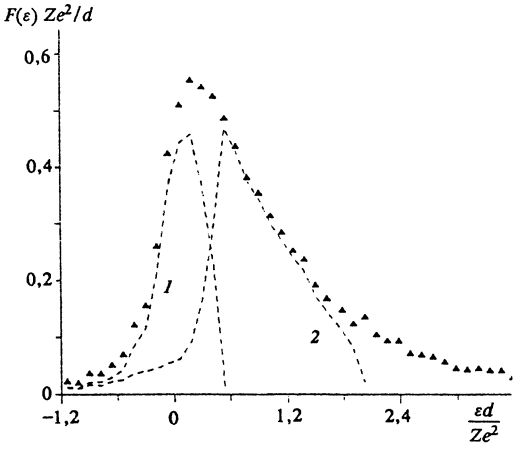

FIG. 2. Distribution function with respect to transverse energy $\varepsilon d/Ze^2$ corresponding to the angular distribution shown in Fig. 1 (triangles). The dashed curves *1* and *2* show the contribution from electrons with departure angles $\vartheta < 0.5\vartheta_L$ and $0.5\vartheta_L < \vartheta < \vartheta_L$, respectively.

in Fig. 1 corresponds to the contribution of channelized particles with $\varepsilon < 0$, which were calculated using (10) and (13).

The effect of the continuous potential on the angular distribution is important even for relatively thick crystals, where $z \gg z_d$. In Fig. 3 we compare the angular distribution of electrons with energies 1 GeV moving along the ⟨111⟩ axis of silicon (the empty triangles) with the case of an amorphous medium. In both cases, the thickness of the target was 200 μm. In the neighborhood of the maximum the difference is about a factor of 2. The numerical simulation for the amorphous medium (the filled triangles) was carried out using the cross section (20). The solid curve in Fig. 3 is a calculation based on the Møller theory using expressions from Ref. 26. In thinner crystals the difference is more significant.[27]

Figures 4 and 5 show the angular distribution and corresponding distribution in transverse energy $\varphi(\varepsilon)$ in phase space for electrons with energies 1 GeV in ⟨110⟩ diamond with thickness 60 μm. Here the dimensionless function $\varphi(\varepsilon)$ is

$$\varphi(\varepsilon, z) = 2\pi m S_0 U_L f(\varepsilon, z) . \qquad (24)$$

The triangular symbols in Figs. 4 and 5 are the result of numerical simulation. The solid and dashed curves in Fig. 4 show the results of calculations using (23) along with the simple model distribution shown in Fig. 5 by the solid and dashed curves respectively. The latter consists of linear portions for small transverse energies $\varepsilon < 0.5\,U_m$ and an exponential tail. For these functions the angular distributions (10), (17), (23) are given by simple but cumbersome formulas. The primary region of transverse energies that determines the behavior of the angular distribution for small angles $\vartheta < 0.5\vartheta_L$ is the region near $\varepsilon = 0$. The behavior of the angular distribution $n(\varepsilon,z)$ is very sensitive to features of the distribution function $f(\varepsilon,z)$ in the transitional region from channelization to quasichannelization (compare the solid and dashed curves in Figs. 4 and 5). These examples show

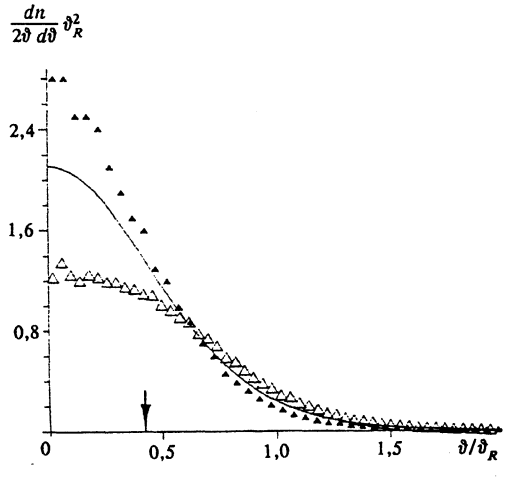

FIG. 3. Comparison of the angular distribution of electrons with $E = 1$ GeV in an oriented crystal with thickness 200 μm (empty triangles) and in an amorphous medium (filled triangles). The solid curve is a calculation using the Møller theory.[26] Here $\vartheta_R = 9.3 \cdot 10^{-4}$ rad; the arrow corresponds to the Linhard angle ϑ_L, and the initial beam divergence was $\Delta = 0.2\vartheta_L$.

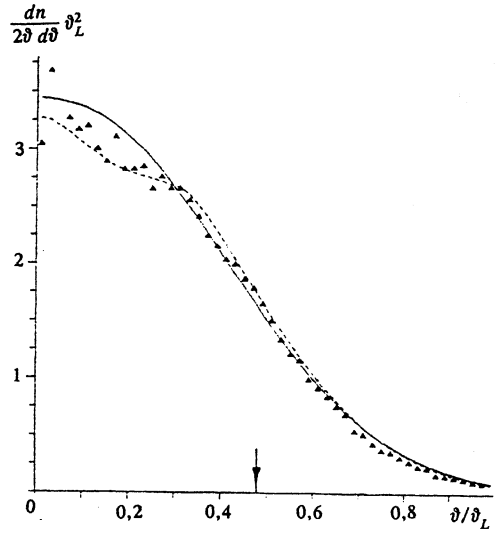

FIG. 4. Angular distribution of electrons with $E = 1$ GeV in ⟨110⟩ diamond with a thickness of 60 μm. The solid and dashed curves correspond to the distribution in phase space represented by the same curves as in Fig. 5; the triangles are the result of numerical simulation. Here $\vartheta_R = 7.7 \cdot 10^{-4}$ rad, $\Delta = 0.2\vartheta_L$.

how the distribution in transverse energy can be recovered from a given angular distribution with a high degree of accuracy.

The existing theories for the motion of electrons in the field of an atomic chain[15-18] allow us to calculate the dechannelization function; however, this is not a directly measurable quantity. We can determine how many particles there are in bound states by measuring the angular distribution. In Table I we show the results of a calculation of the number N_1 of electrons with energies 1 GeV that leave various crystals at angles relative to the axis less than half of the Linhard angle, i.e., $N_1 = N(\vartheta < 0.5\vartheta_L)$. In all cases, the initial divergence of the beam is $\Delta = 0.2\vartheta_L$. According to our calculations the number N_{ch} of electrons in the ⟨110⟩ channel of diamond roughly coincides with the number of electrons with departure angles $\vartheta < 0.5\vartheta_L$, i.e., $N_{ch} \approx N_1$. For ⟨111⟩ silicon the number is $N_{ch} \approx 0.5N_1$, while for ⟨110⟩ germani-

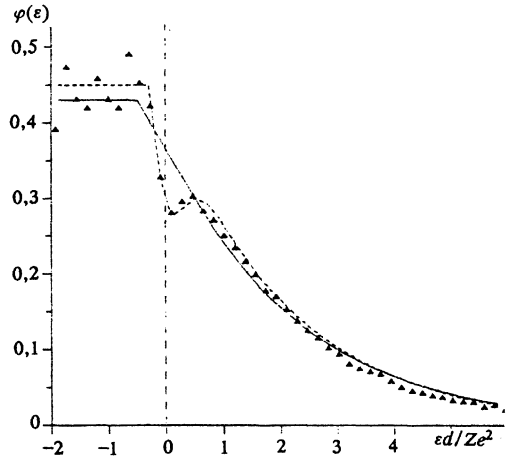

FIG. 5. Distribution functions in phase space (24) corresponding to the angular distributions shown in Fig. 4.

um it is $N_{ch} \approx 0.25 N_1$. These relations depend weakly on the penetration depth of the electrons in the crystal.

Values of the square root of the mean-square angle of deviation $\vartheta_1 = \langle \vartheta^2 \rangle^{1/2}$ are given in Table I. Here

$$\langle \vartheta^2(z) \rangle = \int \vartheta^2 \frac{dn(z)}{2\vartheta d\vartheta} 2\vartheta d\vartheta . \tag{25}$$

All the angles in Table I are given in milliradians. For silicon we also give values of the square root of the mean-square angle of multiple scattering $\vartheta_{am} = \langle \vartheta^2 \rangle_{am}^{1/2}$ for the amorphous medium, which we obtained from a numerical simulation.

5. THE EFFECT OF ELECTROMAGNETIC RADIATION ON THE ANGULAR DISTRIBUTIONS

It is well-known that the motion of electrons and positrons in the field of atomic chains and planes is accompanied by intense electromagnetic radiation. This is a result of quantum transitions between transverse energy levels (the Kumakhov effect).[28] Let us assume that an electron in an initial state with transverse energy $\varepsilon_i(E)$ makes a transition to a state $\varepsilon_f(E-\omega)$, where ω is the photon energy (here and in what follows we set $c = \hbar = 1$). The laws of conservation of energy and conservation of the projection of the momentum in the direction of the chain lead to the following expression for the change $\delta\varepsilon$ in transverse energy due to radiation as a function of the flight angle θ_γ and photon frequency ω:

$$-\delta\varepsilon(\omega) = \frac{\omega}{2\gamma^2} \frac{E}{E-\omega} + \frac{\theta_\gamma^2}{2}\omega . \tag{26}$$

Here $\delta\varepsilon(\omega) \equiv \varepsilon_f(E-\omega) - \varepsilon_i(E)$, $\gamma = (1-v^2)^{-1/2}$ is the Lorentz factor, and the angle θ_γ is measured from the direction of the atomic chain.

There are two interesting limiting cases of Eq. (26). In the dipole approximation, for which the characteristic radiation angle is much larger than the critical channelization angle, i.e., $\vartheta_L \gamma \ll 1$, we may set $\theta_\gamma \approx \gamma^{-1}$ in (26). Then $-\delta\varepsilon \approx \omega\gamma^{-2}$. Averaging this expression with respect to the probability of radiation per unit time $W(\omega)$, we obtain a relation between the total and transverse energy losses:

$$\frac{d\varepsilon}{dt} = \frac{1}{\gamma^2}\frac{dE}{dt} , \tag{27}$$

where

$$\frac{dE}{dt} = -\int \omega W(\omega) d\omega .$$

Analogous results for the dipole case were obtained previously in Refs. 29 and 30.

In the other limiting case of high energies, when $\vartheta_L \gamma \gg 1$, wee may assume that a photon radiates strictly in the direction of motion of the particle. Then the angle θ_γ in (26) may be replaced by the angle between the velocity vector of an electron and the atomic chain $\theta_\gamma \approx \vartheta$. At high energies, i.e., in the hundreds of GeV, and for frequencies $\omega \approx 0.5 E_0$, the first term in (26), which depends only on the electron and photon energies, gives a contribution ~ 1 eV, which is much smaller than the contribution of the second term. Then in this approximation we have

$$-\delta\varepsilon(\omega, r) = \frac{\omega}{E}[\varepsilon - U(r)] , \tag{28}$$

i.e., the change in transverse energy now depends on the point at which radiation of the photon took place.

Averaging Eq. (28) with respect to the probability of emission per unit time, we obtain

$$\left\langle \frac{d\varepsilon}{dt} \right\rangle = \left\langle \frac{\varepsilon - U(r)}{E} \frac{dE}{dt} \right\rangle , \tag{29}$$

where the angle brackets denote averaging over a period of the transverse motion. Equation (29) is well-known in theories of channelization in which energy losses are taken into account.[31]

The approximation (28) was used recently[21-24] to interpret the radiation spectrum of electrons with energies 150–300 GeV in oriented crystals. Equation (28) can be used when the force exerted on an electron by the chain varies insignificantly over the length in which the radiation is generated (the "constant-field approximation").[32,33] In this case the expressions for calculating the probability of synchrotron radiation are valid:[34]

$$W(E, \omega, r) = -\alpha\gamma^{-2}\left[\int_y^\infty \mathrm{Ai}(t)dt + \left(2 + \frac{\omega}{E-\omega}\right)\frac{\mathrm{Ai}'(y)}{y}\right] , \tag{30}$$

TABLE I. Number of electrons N_1 with departure angles $\vartheta < 0.5\vartheta_L$ and the square root of the mean square deflection angle ϑ_1 (in mrad). The beam energy was 1 GeV, with $\Delta = 0.2\vartheta_L$.

element	parameter	penetration depth of electrons into crystal, mm				
		10	20	60	100	200
C	N_1	0,40	0,31	0,165	0,12	0,065
⟨110⟩	ϑ_1	0,30	0,345	0,47	0,55	0,69
Si	N_1	0,43	0,30	0,14	0,10	0,061
⟨111⟩	ϑ_1	0,324	0,40	0,57	0,68	0,88
	ϑ_{am}	0,175	0,23	0,39	0,51	0,70
Ge	N_1	0,34	0,23	0,10	0,07	0,036
⟨110⟩	ϑ_1	0,60	0,74	1,08	1,31	1,74

where

$$y = \left(\frac{\omega}{(E-\omega)\chi(r)}\right)^{2/3}, \quad \chi(r) = |\nabla U| E m^{-3},$$

$$\alpha = 137^{-1}.$$

In what follows we will be interested in the energy distribution function $F(E,t)$ for electrons that leave the crystal. The probability that the sum of the energies of all the photons radiated by a single electron lies between ω and $\omega + d\omega$ is $P(\omega,t)d\omega = F(E_0 - \omega,t)d\omega$, where E_0 is the initial energy of an electron and

$$\int_0^{E_0} P(\omega, t)d\omega = 1.$$

The radiation intensity measured in the experiments will be

$$I(\omega, t) = \omega P(\omega, t). \qquad (30a)$$

We used numerical simulation to calculate the probability distribution $P(\omega,t)$ using the approximations (28) and (30). Figure 6 shows a comparison of our results for the quantity (30a) with the experiments of Ref. 35, whose authors measured the intensity of radiation of electrons having energy 150 GeV in crystals of ⟨110⟩ silicon with thickness 165 and 1400 μm. In Fig. 6 the quantity ω is the total energy of all photons radiated by a single electron. In these calculations we did not take into account the contributions from those electrons for which the total energy of all the radiated photons is smaller than 0.01 E_0; this contribution is not important for the quantity (30a). It is clear from Fig. 6 that for a thin crystal the agreement with experiment is good, whereas for thick crystals the approach discussed here gives an underestimate. The intensity of the radiation shown in Fig. 6 is given in the units of this same quantity for an amorphous medium. The latter is defined as the ratio of the crystal thickness to the radiation length.

The distributions with respect to total energy for electrons leaving the crystal at various angles with respect to the axis are shown in Fig. 7 for electrons with energy 150 GeV in ⟨110⟩ Si with a thickness of 1400 μm. The curves in Fig. 7 correspond to the spectrum of photons shown in Fig. 6 (the solid curve). It is clear that the energy distribution is different for particles departing the crystal at different angles: the larger the energy an electron loses to radiation, the larger the average angle with which it leaves relative to the chain. This is associated with an increase in the critical angle for channelization, and with enhancement of the role played by multiple scattering as the beam energy decreases.

Angular distributions for electrons with energy 150 GeV in Si are shown in Fig. 8 for various thicknesses. It is clear that there is a certain range of angles within which the distribution is almost uniform. Calculations show that this same feature is also encountered in other crystals at these energies.

Radiative attenuation of the transverse energy is clearly apparent in cases where the initial beam has a large angular divergence $\Delta \sim (2\text{–}3)\vartheta_L$. In this case, self-focusing of the beam can occur in a small angular region $\delta\vartheta < 0.5\vartheta_L$ (see Fig. 9). For the case illustrated in Fig. 9, the number of particles in the channel increases significantly with depth. For thicknesses 100, 400, and 600 μm, this number is 1.5, 2.6, and 3.1% respectively.

Equation (28) assumes that the photon is radiated strictly in the direction of the velocity vector. In this case the angle relative to the atomic chain does not change, so that the existence of radiative self-focusing is not *a priori* obvious. In order to consider this question in more detail, let us introduce the electron distribution function $F(\varepsilon,E,t)$ such that

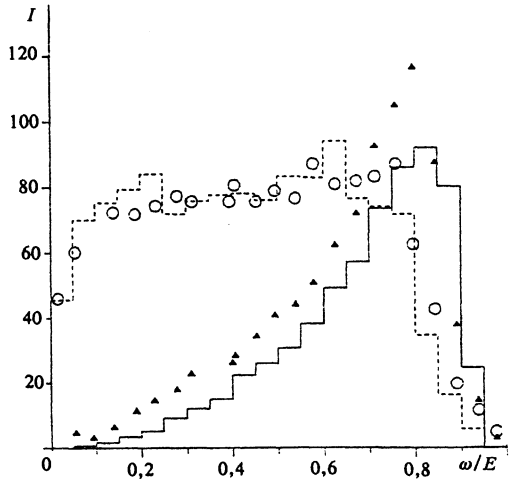

FIG. 6. Intensity of electromagnetic radiation (in units of the ratio of the crystal thickness to the radiation length) for electrons with energies of 150 GeV in ⟨110⟩ silicon. The circles and triangles are experiment[35] for thicknesses of 165 and 1400 μm, while the dashed and solid curves are our calculations for these same thicknesses. The initial beam divergence was $\Delta = 7 \cdot 10^{-6}$ rad.

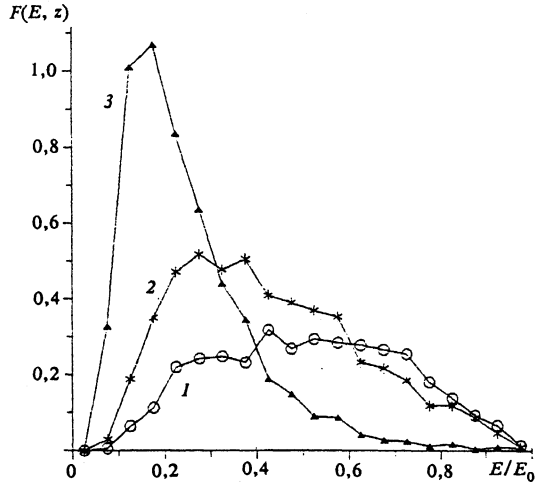

FIG. 7. Total energy distribution function for electrons with energy 150 GeV departing from the crystal at various angles: *1*—$\vartheta < 0.5\vartheta_L$, *2*—$0.5\vartheta_L < \vartheta < \vartheta_L$, *3*—$\vartheta > \vartheta_L$. Here $\vartheta_L = 3.7 \cdot 10^{-5}$ rad. The beam divergence at the input was $\Delta = 7 \cdot 10^{-6}$ rad, the crystal thickness was 1400 μm.

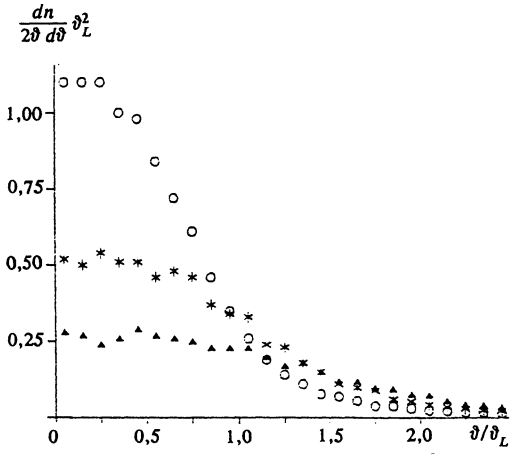

FIG. 8. Angular distribution of electrons with $E = 150$ GeV in ⟨110⟩ silicon with the following thicknesses: O—100 μm (0.07), *—600 μm (0.21), ▲—1400 μm (0.43). Here $\vartheta_R = 1.6\cdot 10^{-5}$ rad, $\Delta = 7\cdot 10^{-6}$ rad. The relative energy losses $\Delta E/E_0$ are given in brackets.

$$\int_{-U_m}^{\infty} d\varepsilon \int_0^{E_0} dE F(\varepsilon, E, t) = 1 .$$

Neglecting multiple scattering, we obtain the following equation for the function $F(\varepsilon,E,t)$, taking the variation of the total and transverse energies to be smooth:

$$\frac{\partial F}{\partial t} + \frac{\partial}{\partial \varepsilon}\left(\frac{\Delta\varepsilon}{\Delta t}\right) F + \frac{\partial}{\partial E}\left(\frac{\Delta E}{\Delta t}\right) F = 0 , \tag{31}$$

where the changes in the total and transverse energies are related by (29). Equation (31) is a limiting case of a more general integral equation. In what follows, we will assume that the photons are radiated close to the chain, and that the energy of an electron varies according to an exponential law, i.e., we will take

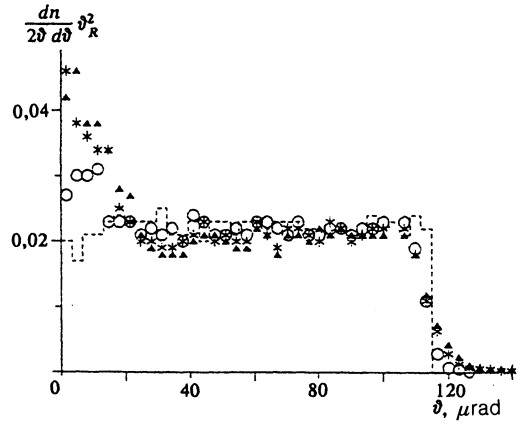

FIG. 9. Angular distribution of electrons with $E = 150$ GeV in ⟨110⟩ silicon with the following crystal thicknesses: O—100 μm (0.032), *—400 μm (0.10), ▲—600 μm (0.14). The divergence of the incident beam $\Delta = 3\vartheta_L$. The dashed curve is the distribution of electrons incident on the crystal. In this plot $\vartheta_R = 1.7\cdot 10^{-5}$ rad.

$$\frac{d\varepsilon}{dt} = \frac{\varepsilon + U_m}{E}\frac{dE}{dt} , \tag{32}$$

where

$$E(t) \equiv E_t = E_0 e^{-\lambda t} . \tag{33}$$

We showed above that if a beam incident on a crystal has a large angle of divergence with a uniform distribution, then the corresponding distribution in phase space is also close to uniform (15). Then the initial distribution in energy space will be

$$F(\varepsilon, E, t=0) = \begin{cases} f_0 r^2(\varepsilon)\delta(E - E_0) , & -U_m < \varepsilon < \varepsilon_0 , \\ 0 , & \varepsilon > \varepsilon_0 , \end{cases} \tag{34}$$

where $\pi r^2(\xi)$ is the area available to an electron with transverse energy ξ, and f_0 is a certain constant.

A solution to Eq. (31) with initial condition (34) is

$$F(\varepsilon, E, t) = \begin{cases} f_0 r^2(\varepsilon_2) e^{\lambda t}\delta(E - E_t) , & -U_m < \varepsilon < \varepsilon_1(t) , \\ f_0 r_0^2 e^{\lambda t}\delta(E - E_t) , & \varepsilon_1(t) < \varepsilon < \varepsilon_m(t) , \end{cases} \tag{35}$$

where E_t is determined by Eq. (33), and

$$\varepsilon_1(t) = U_m(e^{-\lambda t} - 1) , \quad \varepsilon_2(t) = (\varepsilon + U_m)e^{\lambda t} - U_m ,$$
$$\varepsilon_m(t) = (\varepsilon_0 + U_m)e^{-\lambda t} - U_m . \tag{36}$$

The angular distributions can now be computed using, e.g., Eq. (23):

$$n(\vartheta, t)2\pi\vartheta d\vartheta = \int d\varepsilon \int dE F(\varepsilon, E, t) dn(\varepsilon, E, \vartheta) . \tag{37}$$

The simple increase in the number of electrons in the bound state due to radiative damping of the transverse energy does not lead to the appearance of a peak superposed on the uniform angular distribution if the phase-space distribution function $f(\varepsilon,E,t)$ varies smoothly for all ε. The solution (35) shows that a phase-space distribution that is initially uniform can no longer be uniform as the beam penetrates into the crystal. A kink in the behavior of the distribution $f(\varepsilon,E,t)$ as t increases appears at the boundary when $\varepsilon = 0$, which leads to the appearance of this peak.

In Fig. 10 we show the results of calculations using Eq. (23), (35), and (37), for the standard potential (22). The dashed curve is the distribution of particles in an infinite beam with divergence $\Delta = 2\vartheta_L$. It is clear that even a slight energy loss leads to the appearance of a peak.

The self-focusing effects predicted by Kumakhov[36] are due to a somewhat different mechanism which applies to heavy positive particles. The expressions obtained here are also valid for the case where the energy is lost by particles to ionization of target atoms.

6. CONCLUSIONS

Statistical equilibrium in the transverse phase space allows us to introduce a microcanonical distribution. Based on this distribution, it is easy to calculate the angular distributions. Coherent scattering of particles by a continuous potential with conservation of transverse energy leads to a sig-

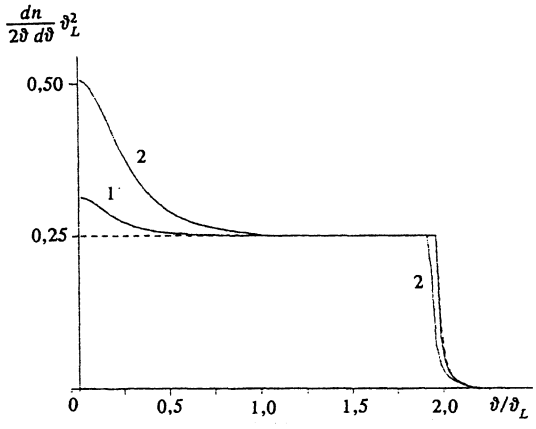

FIG. 10. Initial angular distribution with a beam divergence $\Delta = 2\vartheta_L$, $\lambda = 2.5 \cdot 10^{-4}\ \mu\text{m}^{-1}$ (arrow). Curves *1* and *2* correspond to thicknesses of 100 μm (0.025) and 600 μm (0.14). The relative energy losses are given in brackets.

nificant increase in the mean square angle of deviation compared with an amorphous medium, even in relatively thick crystals.

The canonical phase-space distribution corresponds to a Gaussian angular distribution independent of the form of the atomic chain potential, on which the half-width of the Gaussian distribution depends. If, however, the initial beam has a large angular divergence $\Delta > \vartheta_L$, the corresponding phase-space distribution is also close to uniform.

By measuring the experimental angular distributions, we can reproduce the transverse-energy distribution function to a high degree of accuracy, and also determine the number of electrons found in a bound state.

Radiation of hard photons has a significant effect on the angular distribution for electron energies in the hundreds of GeV. If the initial beam is incident along a crystallographic axis, then electrons departing the crystal at different angles have different distributions in transverse energy. For this case, electrons that have lost a larger fraction of their initial energy to radiation have on the average a larger departure angle with respect to the axis.

Radiation of photons strictly in the direction of the velocity vector is not accompanied by a change in the angle with respect to the atomic chain; however, due to a decrease in the transverse energy, an electron occupies a new position in phase space after radiation with a narrower angular distribution than given by (7). This can lead to the effect of radiative self-focusing, which is manifested as an increase in the number of electrons in comparison with its initial value in the region of angles $\vartheta < 0.5\vartheta_L$, if the incident beam has a large angular divergence $\Delta \sim (2\text{–}3)\,\vartheta_L$.

The author is grateful to Professor J. Linhard, who directed his attention to the special role of the canonical distribution, and also to his colleagues in the city of Århus: I.-U. Anderson, V. A. Ryabov, and E. Uggerhoj for useful discussions of the problem treated here. The author is also grateful to Professor Kumakhov for a discussion of the self-focusing effect.

[1] W. T. Scott, Rev. Mod. Phys. **35**, 231 (1963).
[2] J. Linhard, Kgl. Dan. Selsk. Mat. Fys. Medd. **34**(14) (1964).
[3] V. V. Beloshitskiy and M. A. Kumakhov, Fiz. Tverd. Tela (Leningrad) **15**, 1688 (1973) [Sov. Phys. Solid State **15**, 1019 (1973)].
[4] I. A. Golovchenko, Phys. Rev. B **13**, 4672 (1976).
[5] V. I. Telegin, A. M. Kanloev, and F. R. Kungurov, Zh. Tekh. Fiz. **61**, 117 (1991) [Sov. Phys. Tech. Phys. **36**, 192/317? (1991)].
[6] V. V. Kudrin and S. A. Vorobiev, Rad. Effects **26**, 119 (1975).
[7] A. Neufert, U. Schiebel, and G. Clausnitzer, Rad. Effects **26**, 49 (1975).
[8] M. A. Kumakhov, Usp. Fiz. Nauk **115**, 427 (1975) [Sov. Phys. Usp. **18**, 203 (1975)].
[9] S. M. Darlinian and S. T. Ispirian, Phys. Status Solidi B **96**, 835 (1979).
[10] J. A. Ellison and S. T. Picraux, Phys. Rev. B **18**, 1028 (1978).
[11] V. V. Beloshitsky and Ch. G. Trikalinos, Rad. Effects **56**, 71 (1981).
[12] M. A. Kumakhov, Rad. Effects **26**, 43 (1975).
[13] E. Bonderup, H. Esbensen, J. U. Andersen, and H. E. Schiott, Rad. Effects **12**, 261 (1972).
[14] V. V. Beloshitskiy and M. A. Kumakhov, Zh. Eksp. Teor. Fiz. **66**, 1783 (1974) [Sov. Phys. JETP **39**, 876 (1974)].
[15] V. V. Beloshitskiy and M. A. Kumakhov, Zh. Eksp. Teor. Fiz. **82**, 462 (1982) [Sov. Phys. JETP **55**, 265 (1982)].
[16] V. I. Telegin and M. Kh. Khokonov, Zh. Eksp. Teor. Fiz. **83**, 260 (1982) [Sov. Phys. JETP **56**, 142 (1982)].
[17] V. V. Beloshitskiy, M. A. Kumakhov, and V. A. Ryabov, Zh. Eksp. Teor. Fiz. **87**, 878 (1984) [Sov. Phys. JETP **60**, 498 (1984)].
[18] A. Kh. Khokonov and M. Kh. Khokonov, Zh. Tekh. Fiz. **59**, 163 (1989) [Sov. Phys. Tech. Phys. **34**, 1058 (1989)].
[19] M. Kh. Khokonov and F. K. Tuguz, Zh. Tekh. Fiz. **59**, 77 (1989) [Sov. Phys. Tech. Phys. **34**, 1271 (1989)].
[20] N. Bohr, Kgl. Dan. Selsk. Mat. Fys. Medd. **18**(8) (1948).
[21] Yu. V. Kononets and V. A. Ryabov, Pis'ma Zh. Eksp. Teor. Fiz. **48**, 333 (1988) [JETP Lett. **48**, 364 (1988)].
[22] Yu. V. Kononets and V. A. Ryabov, Nucl. Inst. Methods B **48**, 269 (1990).
[23] Yu. V. Kononets and V. A. Ryabov, Nucl. Inst. Methods B **48**, 274 (1990).
[24] V. V. Beloshitskiy, M. A. Kumakhov, and A. Kh. Khokonov, Nucl. Inst. Methods B **62**, 207 (1991).
[25] P. A. Doyle and P. S. Turner, Acta Cryst. A **24**, 390 (1968).
[26] H. A. Bethe, Phys. Rev. **89**, 1256 (1953).
[27] M. Kh. Khokonov, Pis'ma Zh. Eksp. Teor. Fiz. **56**, 349 (1992) [JETP Lett. **56**, 333 (1992)].
[28] M. A. Kumakhov, Phys. Lett. A **57**, 17 (1976).
[29] M. A. Kumakhov and R. Wedell, Phys. Status Solidi B **92**, 65 (1979).
[30] V. A. Bazylev and N. K. Zhevago, Zh. Eksp. Teor. Fiz. **77**, 1267 (1979) [Sov. Phys. JETP **50**, 637 (1979)].
[31] V. V. Beloshitskiy and M. A. Kumakhov, Zh. Eksp. Teor. Fiz. **62**, 1144 (1972) [Sov. Phys. JETP **35**, 605 (1972)].
[32] J. C. Kimball and N. Cue, Phys. Rep. **125**, 68 (1985).
[33] V. N. Baier, V. M. Katkov, and V. M. Strkhovenko, Phys. Lett. A **114**, 511 (1986).
[34] V. B. Beresteskii, E. M. Lifshits, and L. P. Pitaevskii, *Quantum Electrodynamics*, 2nd ed., Pergamon, Oxford (1982).
[35] R. R. Medenwalt, S. P. Møller , S. Tang-Peterson, E. Uggerhoj *et al.*, Phys. Lett. B **242**, 517 (1990).
[36] M. A. Kumakhov, Pis'ma Zh. Tekh. Fiz. **14**, 112 (1988) [Sov. Tech. Phys. Lett. **14**, 50 (1988)].

Translated by Frank J. Crowne